Thermomechanical model to assess stresses developed during elevated-temperature cleaning of coated optics

H. P. H. Liddell,[1,2,*] J. C. Lambropoulos,[1] and S. D. Jacobs[1]

[1]Laboratory for Laser Energetics, University of Rochester, 240 E. River Road, Rochester, New York 14623, USA

[2]Currently at: Energetics Incorporated, 901 D Street S.W., Suite 100, Washington DC 20024, USA

*Corresponding author: hliddell@energetics.com

Received 21 May 2014; revised 28 July 2014; accepted 29 July 2014;
posted 29 July 2014 (Doc. ID 212516); published 4 September 2014

A thermomechanical model is developed to estimate the stress response of an oxide coating to elevated-temperature chemical cleaning. Using a hafnia–silica multilayer dielectric pulse compressor grating as a case study, we demonstrate that substrate thickness can strongly affect the thermal stress response of the thin-film coating. As a result, coatings on large, thick substrates may be susceptible to modes of stress-induced failure (crazing or delamination) not seen in small parts. We compare the stress response of meter-scale optics to the behavior of small-scale test or "witness" samples, which are expected to be representative of their full-size counterparts. The effects of materials selection, solution temperature, and heating/cooling rates are explored. Extending the model to other situations, thermal stress results are surveyed for various combinations of commonly used materials. Seven oxide coatings (hafnia, silica, tantala, niobia, alumina, and multilayers of hafnia–silica and alumina–silica) and three glass substrates (BK7, borosilicate float glass, and fused silica) are examined to highlight some interesting results.

OCIS codes: (310.6845) Thin film devices and applications; (160.4670) Optical materials; (310.4925) Other properties (stress, chemical, etc.).

http://dx.doi.org/10.1364/AO.53.005865

1. Introduction

During the development of processing techniques for large optics, it is not always possible to test new processing methods on full-size parts because of cost and practicality limitations. Instead, small-scale test pieces are used to learn about a material's response to a treatment (defect production, stress failure, etc.) before committing to the process for the large part. Small samples may also accompany full-scale parts through manufacturing steps as "witnesses" to the fabrication processes used. Witness optics may be subjected to postproduction inspection and analysis in place of the full-size product, which may be too large and unwieldy to undergo some analyses. To ensure the validity of results in extension to larger parts, test and witness samples must be representative of their full-scale counterparts.

As a case study, we consider the chemical cleaning processes used to strip photoresist and other residues from large multilayer-dielectric (MLD) pulse compressor gratings following lithographic fabrication. At the Laboratory for Laser Energetics, hafnia–silica MLD gratings are used for pulse compression in the OMEGA EP Laser System's two ultrashort-pulse beamlines. Each grating segment is 47 cm wide, 43 cm tall, and 10 cm thick. The final phase in the production of these large optics is a cleaning step that must completely remove contaminant materials from the grating surface, including a thick layer of baked-on organic photoresist [1,2]. OMEGA EP

1559-128X/14/265865-14$15.00/0

gratings are cleaned by spraying a heated acid piranha solution (a mixture of hydrogen peroxide and sulfuric acid) over the coated side of the grating. The piranha spray station is depicted schematically in Fig. 1, which shows a full-size OMEGA EP grating being cleaned along with several witness parts. Witness optics (typically 9-mm-thick, 100-mm-diam wafers) are subjected to diagnostic tests in place of the full-size product, including microscopy and laser-induced damage threshold measurement.

The acid piranha solution is widely used to clean delicate MLD pulse-compressor gratings because it is a highly efficient, effective stripper for photoresist and other organic matter [1–5]; however, the acid piranha cleaning process is a source of defects and other problems for the MLD coating. Large-scale puckering [Fig. 2(a)], circular blistering [Fig. 2(b)], tunneling ("telephone-cord") delamination [Fig. 2(c)], and delamination defects (Fig. 2(d); see also Ref. [6]) have been observed on witness and test grating material after chemical cleaning. Delamination failure in layered materials is generally attributed primarily to compressive coating stresses [7]. As a result, understanding the stress response of an MLD coating to elevated-temperature cleaning is essential in determining whether a given optic (coating, substrate, geometry, etc.) and cleaning process (chemical, delivery method, heating profile, etc.) are compatible.

In this work we develop a thermomechanical model to estimate the thermal stresses developed during wet cleaning of a glass substrate with an oxide coating. Coating stress distributions are compared for two substrate thicknesses: a 100-mm-thick substrate, representative of a full-size OMEGA EP grating or other meter-scale optic, and a 10-mm-thick substrate, representative of a small test or witness piece. The effects of substrate material and size, cleaning solution temperature, and heating and cooling rates are examined. Results of this analysis are used to establish the effectiveness of witness/test material in predicting the behavior of a meter-scale coated optic during elevated-temperature chemical cleaning. We also identify modifications that could be made to the cleaning process to mitigate the risk of stress-induced failure. While this paper focuses on a hafnia–silica MLD grating as a case study, similar processing of coated optics may be encountered in a variety of other wet-cleaning and manufacturing applications. The thermomechanical model is extended to other commonly used substrate and oxide coating

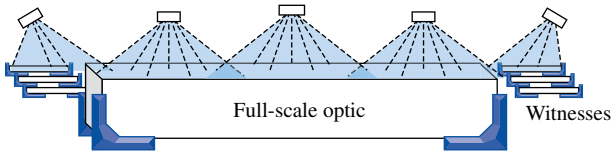

Fig. 1. Schematic illustrating chemical cleaning of a full-size OMEGA EP grating and several witness parts.

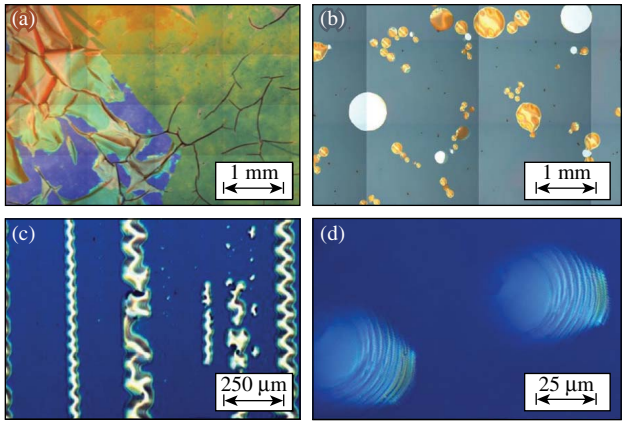

Fig. 2. Examples of coating failure on MLD grating samples observed after elevated-temperature chemical cleaning: (a) buckling of the coating on a plasma-ion-assisted deposition (PIAD) grating; (b) circular delamination on a reactive-evaporation (RE) grating; (c) telephone-cord delamination on a PIAD grating; and (d) delamination defects on a RE grating.

combinations in Section 4.D to identify and explore some interesting trends.

2. Theory

Two situations were considered in the thermal analysis: a finite-plate model, in which the substrate is assumed to occupy a finite thickness L, and a semi-infinite half-space model, in which the substrate is assumed to be thermally thick. The geometry, coordinate system and assumptions involved in the two models are illustrated in Figs. 3(a) and 3(b), respectively. For both models, we make the following assumptions: (1) the heat conduction equation is satisfied; (2) the temperature in the substrate $T(x,t)$ depends on depth x and time t only; (3) the cleaning solution follows a controllable, piecewise-defined temperature profile $T_p(t)$ that includes only linear phases; (4) chemicals flow over the coated side of the optic, leading to convection with the heated solution at the free surface where $x = 0$; and

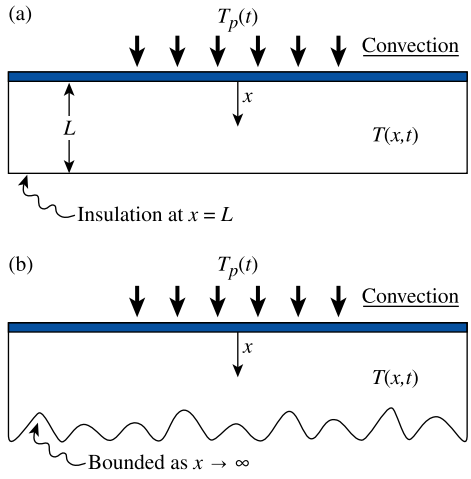

Fig. 3. Problem geometries and assumptions for (a) finite-plate and (b) semi-infinite half-space heat transfer models.

(5) the presence of the thin-film coating has no effect on heat transfer through the substrate. In the finite-plate model, zero heat flux is imposed at the bottom surface where $x = L$. For the semi-infinite half-space, the temperature is only required to be bounded as $x \to \infty$. Note that assumption (2) implies that we are solving the heat conduction equation in one spatial dimension only: the substrate temperature is assumed to be laterally homogenous [$T(x,y,z,t) = T(x,t)$] and edge effects are assumed to be negligible. Assumption (4) implies that we are exclusively considering the case of "one-sided" cleaning, including situations in which chemicals are sprayed or flowed over the coated surface, but excluding situations in which the back side of the optic is exposed to the heated chemical, such as submersion into a bath.

In the next two sections, we solve the heat conduction equation to find the time-dependent temperature distribution in the substrate $T(x,t)$ for each case. Only the semi-infinite half-space problem as described above can be solved in closed form, whereas the finite-plate model provides a better representation of most typical substrate geometries. The validity of the two models for practical substrate geometries is discussed in Section 3.C.

A. Finite-Plate Model

The one-dimensional heat conduction equation is given by

$$\frac{\partial^2 T}{\partial x^2} = \frac{1}{D}\frac{\partial T}{\partial t}, \tag{1}$$

where $T = T(x,t)$ is the temperature in the substrate and D is the thermal diffusivity of the substrate material (assumed independent of temperature). The appropriate boundary conditions (BCs) for the finite plate are convection with the cleaning solution at the coated surface ($x = 0$) and zero heat flux at the bottom of the substrate ($x = L$):

$$-k\frac{\partial T}{\partial x}(0,t) = -h[T(0,t) - T_p(t)], \tag{2}$$

$$\frac{\partial T}{\partial x}(L,t) = 0, \tag{3}$$

where k is the thermal conductivity of the substrate, h is the heat transfer coefficient, and $T_p(t)$ is the temperature of the piranha solution. The initial condition for the problem is

$$T(x,0) = T_0(x). \tag{4}$$

Nondimensionalizing with a new spatial variable $\hat{x} = 1 - x/L$, the problem becomes

$$\begin{aligned}
&\frac{\partial^2 T}{\partial \hat{x}^2} = \frac{L^2}{D}\frac{\partial T}{\partial t},\\
&T(\hat{x},0) = T_0(x),\\
&\frac{\partial T}{\partial \hat{x}}(1,t) + \frac{hL}{k}T(1,t) = \frac{hL}{k}T_p(t),\\
&\frac{\partial T}{\partial \hat{x}}(0,t) = 0,
\end{aligned} \tag{5}$$

where in the new coordinate system, $\hat{x} = 0$ at the bottom of the substrate and $\hat{x} = 1$ at the coated surface. This nonhomogeneous problem is solved (see, e.g., Boley and Weiner [8]) by breaking the temperature $T(\hat{x},t)$ into steady-state and transient parts:

$$T(\hat{x},t) = T_s(\hat{x},t) + u(\hat{x},t). \tag{6}$$

The steady-state solution $T_s(\hat{x},t)$ must satisfy the partial differential equation (PDE) and both BCs given in Eq. (5). Recall that a desired feature of our model was that the chemical temperature profile $T_p(t)$ can be piecewise-defined as a series of linear phases. At this point, we consider only the first phase of this temperature history and assume a linear time dependence such that the temperature profile is given by $T_p(t) = T_{p0} + r_h t$, where r_h is the heating rate. [We account for the complete piecewise temperature profile in the final model (see Section 3.A).] It can be readily verified that a solution for $T_s(\hat{x},t)$ that satisfies the PDE and both BCs is

$$\begin{aligned}
&T_s(\hat{x},t) = C_1\hat{x}^2 + C_2 t + C_3,\\
&C_1 = \frac{L^2 r_h}{2D},\\
&C_2 = r_h,\\
&C_3 = T_{p,0} - \frac{kLr_h}{hD} - \frac{L^2 r_h}{2D}.
\end{aligned} \tag{7}$$

The problem for $u(\hat{x},t)$ becomes

$$\begin{aligned}
&\frac{\partial^2 u}{\partial \hat{x}^2} - \frac{L^2}{D}\frac{\partial u}{\partial t} = 0,\\
&\frac{\partial u}{\partial \hat{x}}(1,t) + \frac{hL}{k}u(1,t) = 0,\\
&\frac{\partial u}{\partial \hat{x}}(0,t) = 0,\\
&u(\hat{x},0) = T_0 - T_{p,0} - \frac{L^2 r_h}{2D}\hat{x}^2 + \frac{kLr_h}{hD} + \frac{L^2 r_h}{2D},
\end{aligned} \tag{8}$$

which is a homogeneous PDE with zero BCs and can be solved by separation of the variables, yielding an infinite series solution for temperature in the substrate:

$$
\begin{aligned}
T(\hat{x},t) &= T_s(\hat{x},t) + u(\hat{x},t),\\
T_s(\hat{x},t) &= T_{p,0} + r_h t + \frac{L^2 r_h}{2D}\hat{x}^2 - \frac{kLr_h}{hD} - \frac{L^2 r_h}{2D},\\
u(\hat{x},t) &= \sum_{n=1}^{\infty} A_n \cos(\lambda_n \hat{x}) \exp\left(-\frac{\lambda_n^2 D}{L^2} t\right),\\
A_n &= \left\{2\left(T_0 - T_{p,0} + \frac{kLr_h}{hD}\right)\sin(\lambda_n) - 2\frac{L^2 r_h}{D\lambda_n^2}\right.\\
&\quad \left.\times [\lambda_n \cos(\lambda_n) - \sin(\lambda_n)]\right\}/\lambda_n + \cos(\lambda_n)\sin(\lambda_n),
\end{aligned}
\tag{9}
$$

where eigenvalues λ_n are solutions to the transcendental equation $\lambda_n \tan(\lambda_n) = hL/k$ for $n = \{1, 2, 3, \ldots\}$.

B. Semi-Infinite Half-Space Model

The semi-infinite half-space problem is defined identically to the finite-plate problem [Eqs. (1)–(4)] except for the BC at $x = L$, which is replaced by the requirement that substrate temperature be bounded for large x. Defining a new variable $\hat{T}(x,t) = T(x,t) - T_0$, the problem becomes

$$
\begin{aligned}
&\frac{\partial^2 \hat{T}}{\partial x^2} = \frac{1}{D}\frac{\partial \hat{T}}{\partial t},\\
&\hat{T}(x,0) = 0,\\
&\frac{\partial \hat{T}}{\partial x}(x,0) - \frac{h}{k}\hat{T}(0,t) = \frac{h}{k}[T_0 - T_p(t)].
\end{aligned}
\tag{10}
$$

We transform the time variable using a Laplace transform such that the substrate and piranha solution temperatures are given by $U(x,s) = \mathcal{L}[\hat{T}(x,t)]$ and $U_p(s) = \mathcal{L}[T_p(t)]$, respectively. The transformed problem is an ordinary differential equation (ODE) in $U(x,s)$:

$$
\frac{\mathrm{d}^2 U}{\mathrm{d}x^2}(x,s) = \frac{s}{D}U(x,s), \tag{11}
$$

$$
\frac{\mathrm{d}U}{\mathrm{d}x}(0,s) - \frac{h}{k}U(0,s) = \frac{hT_0}{ks} - \frac{h}{k}U_p(s), \tag{12}
$$

which has the general solution

$$
U(x,s) = C_1 \exp\left(x\sqrt{s/D}\right) + C_2 \exp(-x\sqrt{s/D}), \tag{13}
$$

where C_1 and C_2 are constants to be determined. Since the temperature of the substrate must be bounded as $x \to \infty$, the constant C_1 vanishes. Applying the convection BC [Eq. (12)] to solve for C_2, we find that the solution for $U(x,s)$ is given by

$$
U(x,s) = \frac{h}{k}\left[\frac{U_p(s) - T_0/s}{\sqrt{s/D} + h/k}\right]\exp\left(-x\sqrt{\frac{s}{D}}\right). \tag{14}
$$

As in the previous section, we assume that the piranha solution follows the linear temperature profile $T_p(t) = T_{p,0} + r_h t$. In s space, the transformed piranha solution temperature is given by $U_p(s) = (T_{p,0}/s) + (r_h/s^2)$. Substituting this expression into Eq. (14) and rearranging,

$$
U(x,s) = \left[\frac{\frac{h\sqrt{D}}{k}\exp\left(-\frac{x}{\sqrt{D}}\sqrt{s}\right)}{\sqrt{s} + \frac{h\sqrt{D}}{k}}\right]\left(\frac{T_{p,0}}{s} + \frac{r_h}{s^2} - \frac{T_0}{s}\right). \tag{15}
$$

To determine the inverse Laplace transform $\hat{T}(x,t) = \mathcal{L}^{-1}[U(x,s)]$ of Eq. (15), we use partial fractions to decompose the expression into a sum of simpler functions. The result of these manipulations is

$$
\begin{aligned}
\hat{T}(x,t) &= \left[T_{p,0} - T_0 + r_h\left(\frac{k}{h\sqrt{D}}\right)^2\right]L_1(x,t)\\
&\quad + r_h L_2(x,t) - \frac{r_h k}{h\sqrt{D}}L_3(x,t),
\end{aligned}
\tag{16}
$$

where

$$
\begin{aligned}
L_1 &= \mathcal{L}^{-1}\left[\frac{\frac{h\sqrt{D}}{k}\exp\left(-\frac{x}{\sqrt{D}}\sqrt{s}\right)}{s\left(\sqrt{s} + \frac{h\sqrt{D}}{k}\right)}\right],\\
L_2 &= \mathcal{L}^{-1}\left[\frac{1}{s^2}\exp\left(-\frac{x}{\sqrt{D}}\sqrt{s}\right)\right],\\
\text{and}\quad L_3 &= \mathcal{L}^{-1}\left[\frac{1}{s^{3/2}}\exp\left(-\frac{x}{\sqrt{D}}\sqrt{s}\right)\right].
\end{aligned}
$$

The inverse transforms L_1, L_2, and L_3 are available in published tables (see Ref. [9]). Returning to the temperature $T(x,t)$, the temperature in the substrate can be expressed in closed form:

$$
\begin{aligned}
T(x,t) &= T_0 - \frac{\exp\left(-\frac{x^2}{4Dt}r_h\sqrt{t}\right)(2k + hx)}{h\sqrt{\pi}\sqrt{D}} + \frac{1}{2h^2 D}\\
&\quad \times \left(\{2k^2 r_h + 2hkr_h x + h^2[r_h x^2\right.\\
&\quad \left. + 2D(r_h t - T_0 + T_{p,0})]\} \times \operatorname{erfc}\left(\frac{x}{2\sqrt{tD}}\right)\right.\\
&\quad - 2\exp\left[\frac{h(kx + hDt)}{k^2}\right][k^2 r_h + h^2 D(-T_0 + T_{p,0})]\\
&\quad \left. \times \operatorname{erfc}\left(\frac{kx + 2Dht}{2k\sqrt{Dt}}\right)\right).
\end{aligned}
\tag{17}
$$

C. Calculation of Thermal Stresses

Since we have assumed that temperature in the substrate arising from cleaning varies only through the thickness of the optic, it follows that the only nonzero stress component, $\sigma_{\mathrm{sub}}(x,t)$, is parallel to the optic's surface. The function $\sigma_{\mathrm{sub}}(x,t)$ must satisfy the

equations of equilibrium and compatibility and appropriate BCs. We apply Saint Venant's principle BCs (see, e.g., Ref. [10]) by assuming that the force and moment due to σ_{yy} and σ_{zz} are zero over the plate's edges—i.e.,

$$\int_0^L \sigma_{\text{sub}}(x,t)\mathrm{d}x = 0$$

and

$$\int_0^L x\sigma_{\text{sub}}(x,t)\mathrm{d}x = 0.$$

The Saint Venant approximation (shown schematically in Fig. 4) is considered very accurate at distances of at least one plate thickness from the traction-free edges. In the present notation, the solution for $\sigma_{\text{sub}}(x,t)$ is

$$\begin{aligned}\sigma_{yy} &= \sigma_{zz} = \sigma_{\text{sub}}(x,t)\\ &= \frac{\alpha_{\text{sub}}E_{\text{sub}}}{1-\nu_{\text{sub}}}\left[-T(x,t) + \left(\frac{4}{L} - \frac{6x}{L^2}\right)\int_0^L T(x,t)\mathrm{d}x\right.\\ &\quad \left. + \left(\frac{12x}{L^3} - \frac{6}{L^2}\right)\int_0^L xT(x,t)\mathrm{d}x\right], \end{aligned} \tag{18}$$

where α_{sub}, E_{sub}, and ν_{sub} are the coefficient of thermal expansion (CTE), Young's modulus, and Poisson ratio for the substrate material, respectively.

Two expressions for $T(x,t)$ were derived in the preceding section based on finite-plate and semi-infinite half-space models of the substrate's geometry. These expressions were substituted into Eq. (18) to determine the thermal stress distribution in the substrate. The integrals

$$\int_0^L T(x,t)\mathrm{d}x$$

and

$$\int_0^L xT(x,t)\mathrm{d}x$$

could be calculated directly in both cases, resulting in an infinite series solution for the finite-plate model and a closed-form solution for the semi-infinite half-space. A similar methodology was used to find the stresses in the thin-film coating at $x = 0$, which depend only on time t:

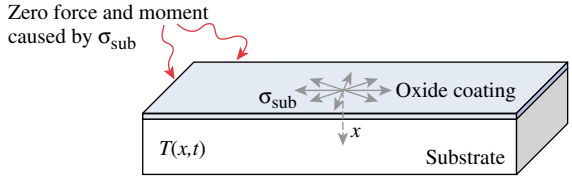

Fig. 4. Schematic illustration of Saint Venant's principle BCs.

$$\begin{aligned}\sigma_{\text{ctg}}(t) = \frac{\alpha_{\text{sub}}E_{\text{ctg}}}{1-\nu_{\text{ctg}}}&\left\{\frac{4}{L}\left[\int_0^L T(x,t)\mathrm{d}x\right]_{x=0}\right.\\ &\left. - \frac{6}{L^2}\left[\int_0^L xT(x,t)\mathrm{d}x\right]_{x=0}\right\} - \frac{\alpha_{\text{ctg}}E_{\text{ctg}}}{1-\nu_{\text{ctg}}}T(0,t),\end{aligned} \tag{19}$$

where $\sigma_{\text{ctg}}(t)$ is the thermal stress in the coating and α_{ctg}, E_{ctg}, and ν_{ctg} are the CTE, Young's modulus, and Poisson ratio for the coating material, respectively. $T(x,t)$ is the temperature distribution in the substrate, as before. Note that stresses in both coating and substrate were assumed to be initially zero. As-deposited coating stresses can be significant, and a coating's stress state can change as a coating ages [11–13]. Such stresses, if present, should be algebraically added to these results for a complete estimate of the stress level in a particular coating.

3. Thermomechanical Model

A. Description of Model

The piranha temperature profile $T_p(t)$ was defined piecewise by a continuous series of linear phases. A simple example of a 60°C piranha cleaning process with 60 min heating and cooling ramps and a 30 min soak period is illustrated in Fig. 5.

Temperature distributions $T(x,t)$ arising from the prescribed cleaning protocol were calculated from Eqs. (9) and (17) for the finite-plate and semi-infinite half-space representations of the substrate, respectively. For the finite plate, a 15-term approximation of the infinite series solution was used. Each phase in the cleaning process was treated separately, with the temperature distribution in the substrate at the conclusion of the previous phase being used as the initial condition for calculations in the following phase. Thermal stresses in the substrate and

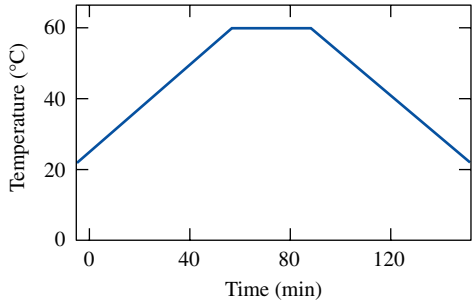

Index (i)	Duration (Δt_i)	Initial temperature	Final temperature
1	60 min	22°C	60°C
2	30 min	60°C	60°C
3	60 min	60°C	22°C

Fig. 5. Sample temperature history $T_p(t)$ for a chemical cleaning process.

coating were calculated using Eqs. (18) and (19), respectively. Codes were developed using the Wolfram *Mathematica* software package to automate these calculations.

B. Material Properties Used in Analysis

Five commonly used oxide single-layer coating materials [alumina (Al_2O_3), hafnia (HfO_2), niobia (Nb_2O_5), silica (SiO_2), and tantala (Ta_2O_5)] are considered in this paper, as well as two MLD coatings [hafnia–silica (HfO_2–SiO_2) and alumina–silica (Al_2O_3–SiO_2)]. Fused silica, BK7, and borosilicate float glass (Schott Borofloat 33) substrates were investigated. Thermoelastic properties of substrate and coating materials are given in Table 1. Thin-film properties were assumed for coating materials, while bulk properties were used for substrates.

C. Comparison of Models for Practical Substrate Geometries

OMEGA EP MLD grating substrates, which are $470 \times 430 \times 100$ mm BK7 slabs, have a low aspect ratio (width to thickness) compared to traditional optics. The large thickness was chosen to reduce wavefront error caused by substrate deformation, whereas the lateral dimensions of the substrate were limited by grating fabrication equipment. Witness and test samples are made with smaller, commercially available substrates, which have much higher aspect ratios than the OMEGA EP grating substrates. Typical samples are fabricated on 100-mm-diameter, 3-or 9-mm-thick round substrates. Samples of 3 mm thickness are broken into smaller pieces for cleaning/chemical exposure experiments (see Ref. [2]). The geometries of OMEGA EP gratings and standard test samples are drawn to scale in Fig. 6.

Saint Venant's principle was used in the application of BCs in the thermal stress model developed in Section 2.C. This approximation is considered excellent at distances at least one plate thickness from the plate's edges, i.e., near the center of the plate [8]. For the 3- and 9-mm-thick substrates, the approximation is a good one over nearly the entire volume of the part, while the fractional region of validity is smaller for the lower-aspect-ratio OMEGA EP grating. In all cases, the model is expected to be accurate near the center of the clear aperture.

To evaluate the validity of the two heat transfer models described in Sections 2.A and 2.B, results were compared for 10-mm-thick (representative of a small test or witness part) and 100-mm-thick (representative of a full-size grating) BK7 substrates using each model. The 60°C piranha temperature history shown in Fig. 5 was assumed arbitrarily. Liu's estimate of $h = 600$ W/m^2·K was used for the heat transfer coefficient of the acid piranha-glass system [21]. Temperature distribution results are shown in Fig. 7, with the finite-plate solution plotted as black ($x = 0$), medium gray ($x = L/2$), and light gray ($x = L$) curves and the semi-infinite half-space solution plotted as dotted black ($x = 0$), dotted medium gray ($x = L/2$), and dotted light gray ($x = L$) curves. The temperature of the piranha solution itself is shown in purple.

The entire 10-mm-thick substrate [Fig. 7(a)] closely followed the temperature profile of the heated chemical. All three temperature curves (corresponding to substrate depths of $x = 0$, $x = L/2$, and $x = L$) calculated using the finite-plate solution were nearly identical to the piranha temperature curve itself. The lateral dimensions of a 10-mm-thick witness or test sample would normally be much larger than the thickness, so the finite-plate model provides a better representation of this substrate geometry; indeed, the semi-infinite half-space model (indicated by dotted curves) led to different results.

In the case of the 100-mm-thick substrate [Fig. 7(b)], a strong temperature gradient through the substrate developed immediately. The coated surface ($x = 0$) quickly responded to temperature changes in the convective fluid, but the back side of the part had a lagging response because heat conduction through the thick glass was slow. The low aspect ratio of the 100-mm-thick OMEGA EP grating substrate suggests that treating it as a half-space might be reasonable, but the plate and half-space models agreed only for early behavior.

Although temperature results were different for the two models, ultimately the choice of one model over the other did not have a large effect on thermal stress calculations. Because optical glasses are insulators, heat transfer through the substrate is slow, and the insulation BC at the back surface of the

Table 1. Thermoelastic Properties of Substrate and Oxide Thin-Film Coating Materials

Material	Young's Modulus E (GPa)	Coefficient of Thermal Expansion α	Poisson Ratio ν	Thermal Diffusivity D (m^2/s)	Thermal Conductivity k (W/m · K)	Ref.
BK7	82.0	8.3×10^{-6}	0.21	5.5×10^{-7}	1.11	[14,15]
Fused silica	72.7	0.52×10^{-6}	0.16	7.5×10^{-7}	1.30	[16]
Borofloat 33	64.0	3.3×10^{-6}	0.20	6.1×10^{-7}	1.20	[17,18]
Al_2O_3	73.0	8.2×10^{-6}	0.22	n/a	n/a	[19]
HfO_2	195.0	3.6×10^{-6}	0.25	n/a	n/a	[19]
Nb_2O_5	130.0	4.9×10^{-6}	0.22	n/a	n/a	[20]
SiO_2	71.4	3.1×10^{-6}	0.17	n/a	n/a	[19]
Ta_2O_5	136.0	4.4×10^{-6}	0.27	n/a	n/a	[20]

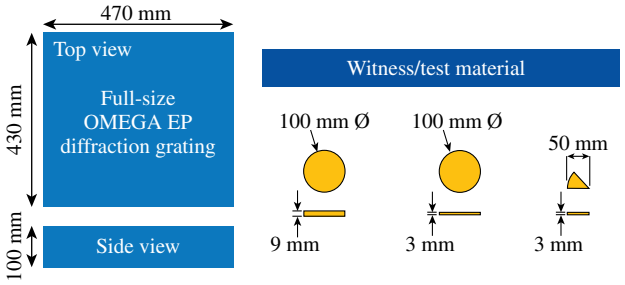

Fig. 6. Dimensions of full-size OMEGA EP diffraction gratings and standard witness and test material (drawn to scale).

optic has little effect on stress calculations at time scales relevant to chemical cleaning. Figure 8 compares thermal stresses calculated using the two models for a BK7 substrate with a hafnia–silica MLD coating subjected to the piranha treatment of Fig. 5. Stress results are discussed in Section 4, but it is clear that the models are in excellent agreement. The finite-plate solution—which intuitively provides a better representation of practical substrate geometries that are thin in comparison with their lateral dimensions—was used for all remaining stress calculations. Note that computation time is much longer for the series solution than for the closed-form half-space solution. Therefore, the semi-infinite half-space solution is quite useful for checking results and performing preliminary calculations.

4. Stress-Modeling Results

A. Coating Stresses Developed in an OMEGA EP Grating

Ashe *et al.* [1] optimized a piranha cleaning process for LLE hafnia–silica MLD gratings in 2007 and reported that a 100°C piranha process led to the best laser-induced damage thresholds, although the authors expressed concerns about thermal shock to the 100-mm-thick OMEGA EP substrate at such

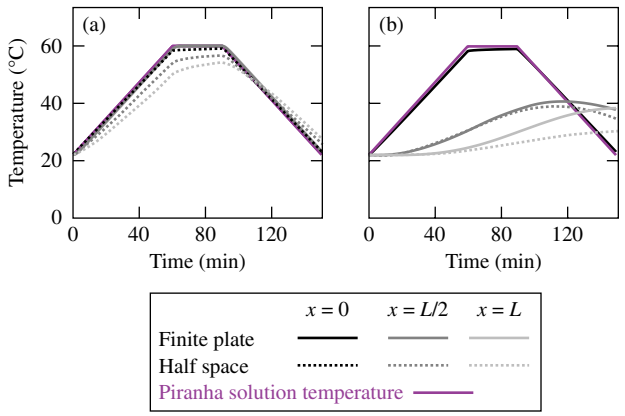

Fig. 7. Solutions to the heat conduction equation for (a) 10-mm-thick and (b) 100-mm-thick BK7 substrates subjected to piranha cleaning at 60°C. The temperature history of the piranha solution is indicated in purple. Finite-plate and half-space solutions for temperature profiles at three depths in the substrate are represented by solid and dotted curves, respectively.

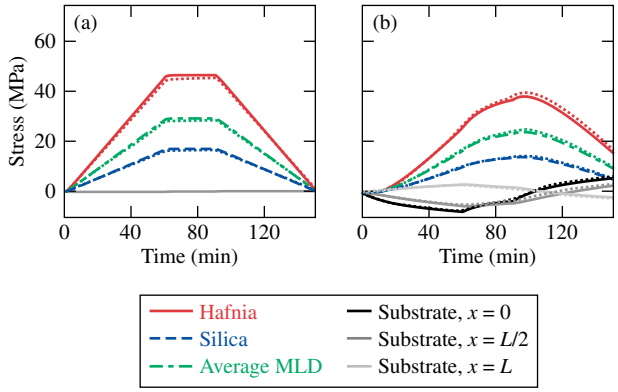

Fig. 8. Thermal stress results for a hafnia–silica MLD coating on (a) 10-mm-thick and (b) 100-mm-thick BK7 substrates, corresponding to the 60°C piranha cleaning considered in Fig. 7. The red and blue curves show the stresses in the individual hafnia and silica layers, while the green curves show the thickness-weighted average film stress (assuming a quarter-wave design). The black and gray curves show the substrate stresses, with black, medium gray, and light gray corresponding to depths of $x = 0$, $x = L/2$, and $x = L$, respectively. Finite-plate solutions are represented by solid and dashed curves, and half-space solutions are represented by dotted curves.

high temperatures. The thermal stresses developed in an MLD grating during piranha cleaning at 100°C (assuming 60 min heating and cooling ramps—the same ramp durations assumed for the 60°C profile considered in the previous section) were calculated using the present model; results are presented in Figs. 9(a) and 9(b) for 10-mm-thick and 100-mm-thick BK7 substrates, respectively.

Substrate stresses were near zero in the 10-mm-thick substrate (ranging from −0.29 to +0.29 MPa) and were significantly higher in the 100-mm-thick substrate (ranging from −15.7 to +11.8 MPa). Using

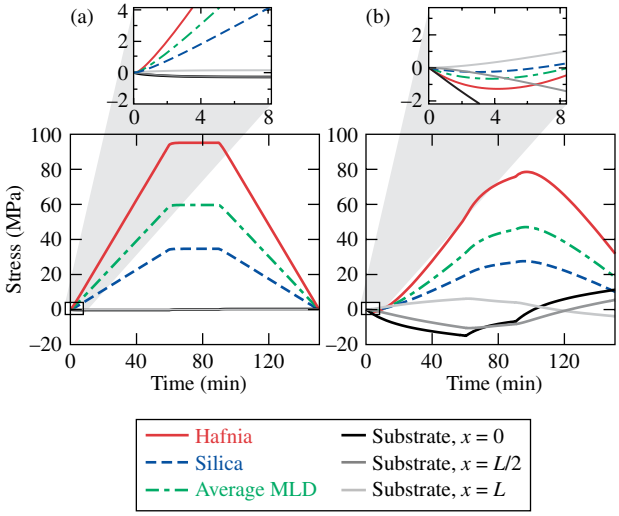

Fig. 9. Thermal stress response of a hafnia–silica coating on (a) 10-mm-thick and (b) 100-mm-thick BK7 substrates subjected to piranha cleaning at 100°C (with a 30 min soak period and 60 min ramp periods for heating and cooling). Inset plots show magnified views of the early behavior in each case.

a fracture toughness approach, the critical flaw size for crack growth is given by [22,23]

$$a_c = \frac{1}{\pi}\left(\frac{K_c}{\sigma_t}\right)^2, \tag{20}$$

where a_c is the depth of an assumed half-penny-shaped crack, K_c is the fracture toughness, and σ_t is the tensile stress. With a fracture toughness of $K_c = 0.82\ \text{MPa}\sqrt{m}$ for BK7 [24], the critical flaw size a_c calculated from Eq. (20) is 1.5 mm. A 11.8 MPa tensile stress would be expected to cause catastrophic substrate fracture in the presence of a larger flaw. The maximum-allowable flaw size could be even smaller if slow crack growth (stress-corrosion cracking) occurs during piranha cleaning [25]. Therefore, substrate fracture is a risk during cleaning at 100°C, as pointed out by Ashe *et al.* [1], but data in Fig. 9 show that coating stress failure is also a possibility. Since BK7 has a higher CTE than the coating, the hafnia–silica coating is forced into tension during elevated-temperature cleaning. The maximum tensile stresses developed in the hafnia–silica coating (calculated as a thickness-weighted MLD average stress) were 59.9 and 49.3 MPa for the 10-mm-thick and 100-mm-thick substrates, respectively. These are significant stress levels, especially considering that RE-deposited coatings are highly susceptible to tensile-stress failure [11,26]. Tensile stresses on the order of ~100 MPa have been known to cause coating fracture [27], a level that could easily be reached during elevated-temperature cleaning of an RE-deposited hafnia–silica MLD coating, which would often already be in tension prior to cleaning [12,13]. Pre-existing stresses should be algebraically added to cleaning-induced stresses to estimate the total stress.

The shape of the thermal stress curve was quite different for the two substrate thicknesses. In the thick-substrate case, the coating stress shifted to a compressive state briefly before becoming tensile; this did not happen in the thin-substrate case. The inset plots in Fig. 9 show magnified views of this early behavior. While the compressive coating stresses were small in magnitude (less than 1 MPa), it is troubling that they were not reflected in the stress response of the representative witness part. Poor representation of a full-scale component's behavior by small witness/test pieces is problematic because cost and practicality limitations preclude cleaning experiments on full-thickness parts. The ability to predict the behavior of a full-size component using inexpensive, small-scale samples before committing to a processing methodology is valuable since results can be used to avoid a process that is likely to cause catastrophic failure in a full-size product.

B. Effect of Substrate Choice

Considering again the case of an MLD grating subjected to a 100°C piranha treatment, the stress responses of a hafnia–silica coating on 10-mm-thick BK7, fused silica, and borofloat substrates are compared in Fig. 10. These results correspond to possible witness or test samples that might be used to represent large-aperture optical components. BK7 is the substrate material used to fabricate OMEGA EP gratings, while fused silica is used for large-aperture MLD gratings in other short-pulse laser systems [12,28]. Borofloat glass was considered because high-quality substrates in witness sizes are readily available. Substrate stresses were near zero in all three cases and are not shown.

The three substrate materials considered are all common optical glasses, but they have different thermal properties: fused silica has an exceptionally low CTE of $\alpha = 0.52 \times 10^{-6}$; borofloat is a low-expansion glass with a CTE of $\alpha = 3.3 \times 10^{-6}$; and BK7 has a CTE of $\alpha = 8.3 \times 10^{-6}$. Since the thin-film coating is adhered to the substrate and has no mechanical stiffness of its own, it is forced to conform to the expansion behavior of the substrate material. As a result, the thermal stress response of the coating depended strongly on the choice of substrate. For a BK7 substrate [Fig. 10(a)], MLD coating stresses shifted tensile as the optic was heated because hafnia and silica layers have lower CTEs than the substrate. Borofloat [Fig. 10(b)] has a comparable CTE to the coating materials (slightly lower than thin-film HfO_2 and slightly higher than thin-film SiO_2), leading to modest overall coating stresses; hafnia layers shifted to a slightly compressive state during heating, and silica layers slightly tensile. Fused silica [Fig. 10(b)] has a lower CTE than the coating materials, so the MLD layers were forced into compression when the optic was heated.

Note that these substrates were not interchangeable: the stress response of a coating on a borofloat substrate was not representative of a BK7 sample, and so on. If thermal stresses are a concern, a witness or test sample must be fabricated with the same materials as the model part. This may seem obvious, but it is important to appreciate, since it can be tempting to use any samples that happen to be available for experiments, especially if they are

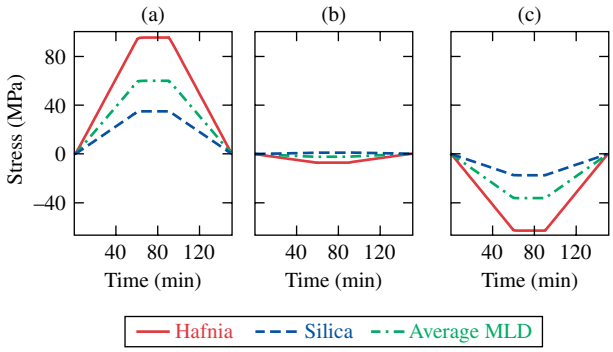

Fig. 10. Stress response of hafnia–silica coating on a 10-mm-thick substrate subjected to piranha cleaning at 100°C (60 min heating and cooling ramps, 30 min soak). Substrate materials were (a) BK7, (b) borofloat, and (c) fused silica.

functionally similar. Care should be taken with such substitutions as a cleaning process that may be consistent and effective for a fused-silica optic could cause equally consistent stress failure in the same coating on BK7. Furthermore, none of these witnesses was representative of the stress response of a full-size, 100-mm-thick BK7 OMEGA EP grating (Fig. 9).

Further probing of this issue by adjusting variables in the thermomechanical model revealed that the effect of the substrate thickness was more important for certain material combinations than for others. For a hafnia–silica coating on BK7, we saw from Fig. 9 that the thermal stress behavior was quite different for the witness and full-size optic. Figure 11 shows results for a borofloat substrate, assuming the same coating and processing history. Like BK7, the use of a borofloat substrate led to substantially different stress responses for the 10-mm-thick and 100-mm-thick parts. The thin substrate [Fig. 11(a)] resulted in near-zero coating stresses, with the average MLD stress remaining small and nominally compressive for the entire processing history (in the range of −2.5 to +0.13 MPa). The 100-mm-thick substrate [Fig. 11(b)], on the other hand, saw an average MLD stress that was compressive for most of the process duration, but shifted tensile during cooling. The range of coating stresses (−10.8 to +6.4 MPa) was also broader in the thick-substrate case. For this choice of substrate, the small-scale test sample would not be predictive of the full-size grating's behavior for any part of the piranha process, since the magnitude and sign of the coating stress depended on substrate thickness.

Figure 12 shows thermal stress results for a fused-silica substrate, again assuming the same processing history and coating materials. When fused silica was used as the substrate, stresses in the coating shifted to a compressive state as the optic was heated because fused silica has a lower CTE than do the coating materials. Unlike the other two substrate materials, the behavior of the thin fused-silica witness [Fig. 12(a)] was almost identical to the thermal stress behavior of the full-size fused-silica optic [Fig. 12(b)]. For a substrate with an extremely low CTE, like fused silica, the first two terms in Eq. (19)—the only terms that depend on substrate thickness—are very small. The third term, which depends only on the coating's thermomechanical properties and the surface temperature, dominates the stress behavior. This does not mean that fused silica is necessarily a "better" choice of substrate than other materials—in fact, compressive coating stresses were significantly higher in the fused-silica case than for either of the other substrate materials considered. However, a fused-silica witness was found to be a better predictor for the behavior of a large fused-silica optic, which is a significant advantage for process development work.

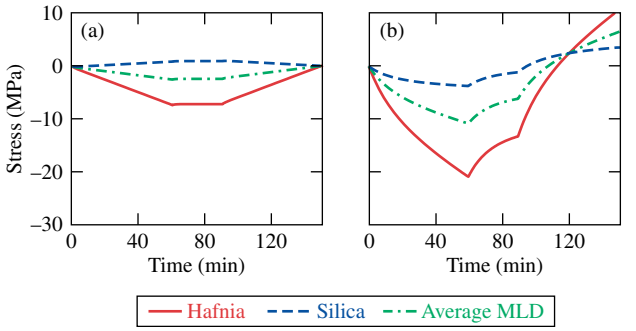

Fig. 11. Thermal stress response of a hafnia–silica coating on (a) 10-mm-thick and (b) 100-mm-thick borofloat substrates subjected to piranha cleaning at 100°C (60 min heating and cooling ramps, 30 min soak).

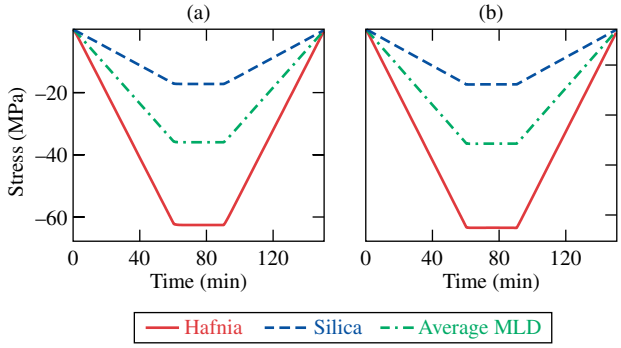

Fig. 12. Thermal stress response of a hafnia–silica coating on (a) 10-mm-thick and (b) 100-mm-thick fused-silica substrates subjected to piranha cleaning at 100°C (60 min heating and cooling ramps, 30 min soak).

C. Piranha Cleaning Process Modifications

In our earlier analysis, we assumed a 100°C cleaning process with 60 min heating and cooling periods and a 30 min soak duration. The piranha spray cleaning station is equipped with a programmable heater, so temperature and heating rate adjustments can be made relatively easily. Using the developed thermomechanical model, the acid piranha temperature profile was varied to identify possible improvements that could be implemented to mitigate coating stresses. In the next two sections we probe the effects of heating rates and soak temperature.

1. *Heating and Cooling Rates*

Heating and cooling rates were varied to study how this parameter affects the temperature distributions and stresses developed during cleaning. Figure 13 shows the temperature distributions in a 100-mm-thick BK7 substrate (i.e., an OMEGA EP grating) for heating and cooling ramp durations of 10, 20, 60, and 120 min. The cleaning processes were otherwise identical to the protocol considered earlier, including a 30 min soak at a maximum temperature of 100°C. When the piranha solution was heated and cooled quickly, the coated surface responded to the rapidly changing piranha solution temperature, but the bulk of the substrate lagged behind because of slow conduction through the thick glass, leading to

large temperature variations through the thickness of the substrate. In the 10 min ramp case [Fig. 13(a)], the back side of the substrate remained almost at room temperature for the entire process. The maximum substrate temperature delta (temperature difference from $x = 0$ to $x = L$) during this process was 74.1°C, which occurred during the soak period ($t = 21.7$ min).

The use of longer heating and cooling ramps reduced the magnitude of temperature gradients developed in the substrate: in the 120 min ramp case [Fig. 13(d)], the maximum temperature delta was 58.6°C (at $t = 120$ min). In this case, the back side of the optic remained hotter than the coated side for most of the cooling process because the piranha solution convectively cooled the front of the optic more quickly than the back side could cool. At the end of the process, the back side of the substrate remained above 60°C, while the coated surface had cooled to room temperature.

Corresponding thermal stress results are shown in Fig. 14 for a hafnia–silica MLD coating. In the case of short 10 min ramps [Fig. 14(a)], coating stresses initially dipped to a compressive state during heating, then shifted to a tensile state during the soak period. A tensile coating stress persisted after the cooling process ended because the bulk of the substrate remained above ambient temperature [see Fig. 13(a)]. These stresses would return to zero once the substrate cooled completely. In the case of 120 min ramps [Fig. 14(d)], coating stresses increased steadily during heating (apart from a very short initial phase) and decreased steadily during cooling.

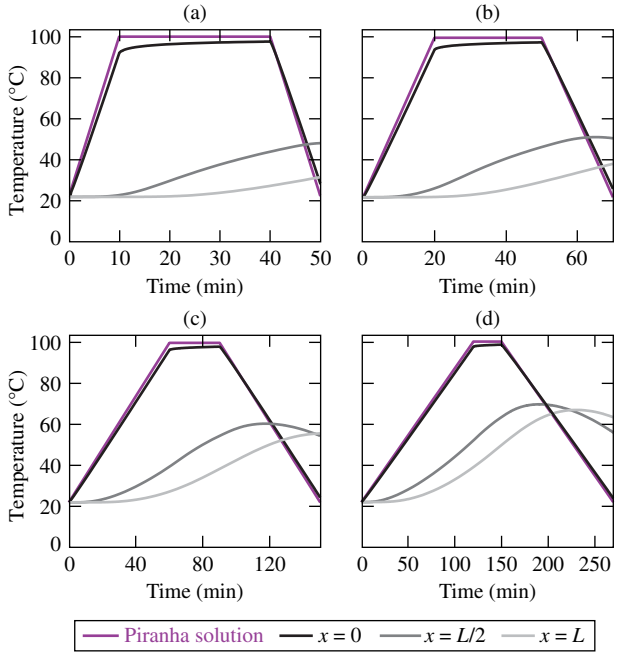

Fig. 13. Temperature distributions in a 100-mm-thick BK7 substrate resulting from piranha cleaning at 100°C with (a) 10, (b) 20, (c) 60, and (d) 120 min heating and cooling ramps. The temperature history of the piranha solution is indicated in purple.

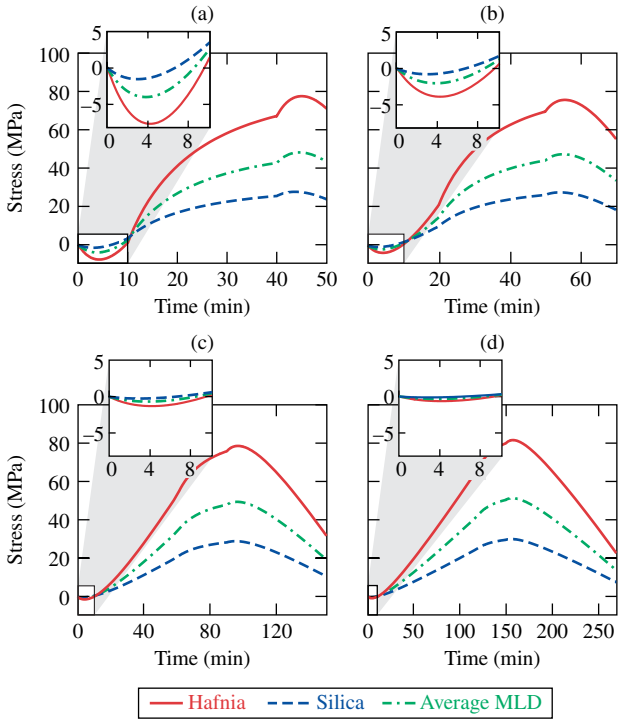

Fig. 14. Thermal stresses in a hafnia–silica MLD coating on a 100-mm-thick BK7 substrate developed during piranha cleaning at 100°C with (a) 10, (b) 20, (c) 60, and (d) 120 min heating and cooling ramps. Corresponding temperature distributions in the substrate are shown in Fig. 13.

Again, a tensile coating stress persisted at the end of the process, but the magnitude of this stress was smaller than in the rapid-heating case. Figures 14(b) and 14(c) show the stress response of the coating for the 20 and 60 min ramps, illustrating the transitional behavior between rapid-heating and slow-heating extremes.

The insets in Fig. 14 show magnified views of coating stresses during initial heating ($0 < t < 10$ min) for each case. For the 10 min ramp (corresponding to a heating rate of 7.8°C/min), the MLD average stress reached a minimum of –4.0 MPa at $t = 3.8$ min. The minimum MLD stress for the 120 min ramp (corresponding to a heating rate of 0.65°C/min) was –0.33 MPa, also at $t = 3.8$ min. While these stresses are relatively small in magnitude, compressive stresses in general are of concern because (1) delamination is a known mode of coating failure in MLD gratings and (2) witness or test samples would not be predictive of this behavior, as discussed in Section 4.A.

While compressive coating stresses in the coating were highest for rapid heating, tensile stresses were indeed highest when the substrate was heated slowly. Coating stress extrema are plotted as a function of the heating/cooling rate in Fig. 15 for substrate thicknesses of 10 and 100 mm. For the 100-mm-thick BK7 substrate, the maximum tensile stress [Fig. 15(a)] decreased from 57.8 to 47.7 MPa as the heating rate increased from 0.1°C/min to

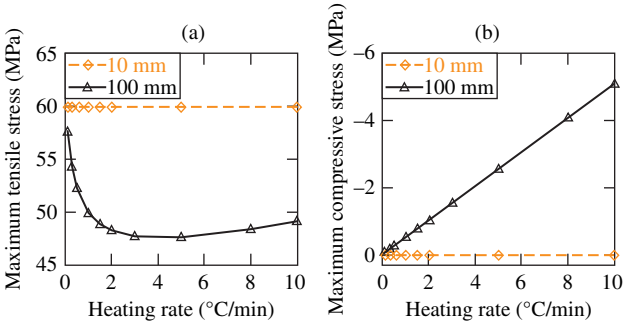

Fig. 15. Dependence of (a) maximum tensile coating stress and (b) maximum compressive coating stress on heating/cooling rate for a hafnia–silica MLD on 10-mm-thick and 100-mm-thick BK7 substrates. A 100°C piranha cleaning process with a 30 min soak was assumed.

5°C/min, while heating rates greater than about 5°C/min led to modest increases in the coating stress. Rates in the range of 3°C/min to 5°C/min (corresponding to 15 to 26 min ramps) minimized tensile stresses. Maximum tensile coating stresses were always higher in the thin-substrate case, indicating that a 10-mm-thick witness provides a conservative prediction of tensile coating failure in a thick optic. Conversely, maximum compressive coating stresses [Fig. 15(b)] were near zero in the thin-substrate case but increased linearly with the heating rate for the thick substrate. Maximum compressive coating stresses corresponding to heating rates of 3°C/min to 5°C/min were in the range of −1.5 to −2.6 MPa.

2. *Soak Temperature*

The most effective method for reducing the magnitude of thermal coating stresses is, as one might expect, to lower the temperature of the cleaning process. The main drawback of this approach is that acid piranha cleaning is generally considered to be most effective at high temperatures [1,3]. Our group has recently developed a low-temperature acid piranha cleaning method for MLD gratings that is effective at temperatures as low as 40°C [2]. Figure 16 shows the temperature distributions in a 100-mm-thick BK7 substrate developed during piranha cleaning at 40°C, 60°C, 80°C, and 100°C (assuming 60 min heating and cooling ramps and a 30 min soak duration). The temperature curve shapes were similar for each temperature, differing mainly in amplitude. The maximum substrate temperature deltas (the maximum instantaneous difference in substrate temperature between $x = 0$ and $x = L$) were 16.0°C, 33.8°C, 51.6°C, and 69.3°C for soak temperatures of 40°C, 60°C, 80°C, and 100°C, respectively. Maxima were observed at $t = 60$ min (the beginning of the soak period) in each case.

Figure 17 shows the corresponding thermal stress results for a hafnia–silica MLD coating. The stress curves had a similar shape for all temperatures, but the magnitude of the thermal stress depended on the soak temperature. The maximum tensile

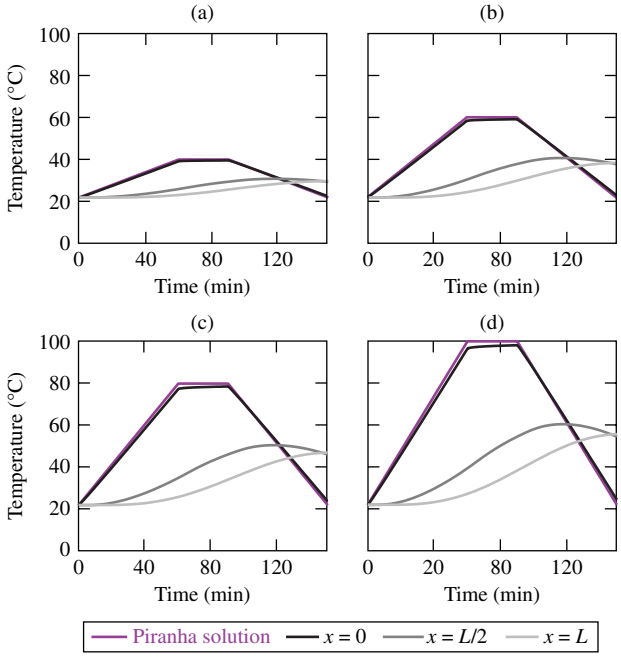

Fig. 16. Temperature distributions in a 100-mm-thick BK7 substrate developed during piranha cleaning at (a) 40°C, (b) 60°C, (c) 80°C, and (d) 100°C, with 60 min heating and cooling ramps and a 30 min soak duration at the maximum temperature.

coating stress (measured as an MLD average) was found to depend linearly on cleaning temperature. This relationship is plotted in Fig. 18 for substrate thicknesses of 10 and 100 mm. For the 100-mm-thick substrate, the maximum tensile coating stress

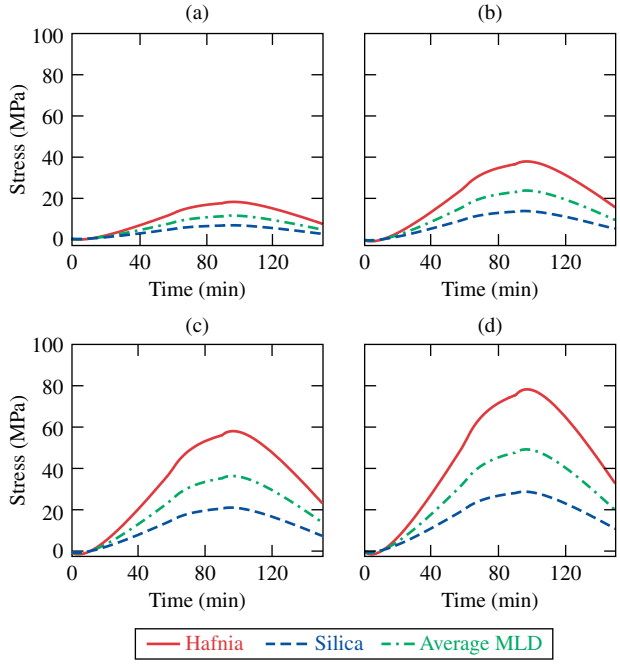

Fig. 17. Thermal stresses developed in a hafnia–silica MLD coating on a 100-mm-thick BK7 substrate during piranha cleaning at (a) 40°C, (b) 60°C, (c) 80°C, and (d) 100°C with 60 min heating and cooling ramps and a 30 min soak period assumed. Corresponding temperature distributions in the substrate are shown in Fig. 16.

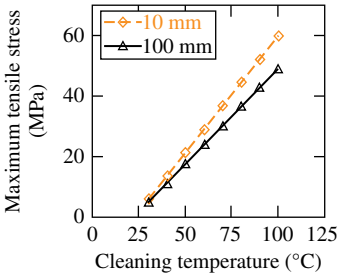

Fig. 18. Relationship between maximum tensile coating stress and cleaning temperature for a hafnia–silica MLD coating on 10-mm-thick and 100-mm-thick BK7 substrates with 60 min heating and cooling ramps and a 30 min soak assumed.

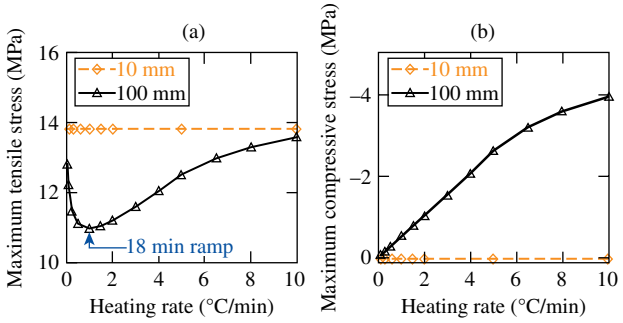

Fig. 19. Dependence of (a) maximum tensile coating stress and (b) maximum compressive coating stress on heating/cooling rate for a hafnia–silica MLD on 10-mm-thick and 100-mm-thick BK7 substrates. A 40°C piranha cleaning process with a 30 min soak was assumed.

encountered during cleaning at 40°C was 11.4 MPa—more than 4× lower than the 49.3 MPa stress encountered during cleaning at 100°C.

3. *Combined Effect of Soak Temperature and Heating Rate*

We showed in Section 4.C.1 that 10 min heating and cooling ramps (corresponding to a heating rate of 7.8°C/min) minimized thermal stresses in the coating for a 100°C cleaning process. A similar analysis was performed to identify the optimal ramp rates for a 40°C cleaning process (the lowest temperature at which effective acid piranha cleaning has been demonstrated [2]), again assuming a 30 min soak period. The relationships between stress maxima and heating rate for the 40°C process are presented in Fig. 19. For this temperature, heating rates in the range of 0.5°C/min to 1.5°C/min minimized tensile coating stresses. Using the optimal heating rate of 1°C/min (corresponding to 18 min heating and cooling ramps), the maximum compressive and tensile coating stresses encountered during cleaning were −0.51 and 11.0 MPa, respectively. Stresses of these magnitudes would not be expected to cause catastrophic coating failure.

D. Extensions to Other Coatings and Substrate Materials

As an extension to the OMEGA EP grating case study, the thermomechanical model developed in this paper was used to compare the thermal stress responses of various combinations of oxide coatings and substrates that are commonly used in laser optics. Table 2 shows the maximum tensile and maximum compressive stresses computed for the cases considered. The usual sign convention of positive tensile stresses and negative compressive stresses has been used. Water ($h = 3000$ W/m^2·K [21]) was used as the convective fluid in calculations for generality, and the 60°C rinse-chemical temperature profile of Fig. 1 was assumed arbitrarily. Material properties were given in Table 1.

General trends in the data were observed for all cases considered. For thin substrates, coating stresses were generally either positive (tensile) or negative (compressive) for the entire processing history, depending on the difference in CTE between the substrate and coating. For thick substrates, both compressive and tensile coating stresses were often encountered. If the coating had a high CTE compared to the substrate, the coating stress was compressive for most of its history but shifted tensile during cooling. If the substrate's CTE was higher than that of the coating, the film stress shifted briefly to a compressive state, then became tensile (as seen in the example of a hafnia–silica MLD coating on thick BK7 glass). We conclude from these modeling results that coating stresses are highly dependent on substrate thickness in most cases. Therefore, the stress response of a small witness sample may not be

Table 2. Maximum Compressive (Negative) and Maximum Tensile (Positive) Thermal Coating Stresses Resulting from Wet Cleaning at 60°C for Several Coating–Substrate Combinations

	Substrate					
	Maximum Compressive/Maximum Tensile Stress in Thin-Film Coating (MPa)					
Coating	BK7 10 mm	BK7 100 mm	BF 10 mm	BF 100 mm	FS 10 mm	FS 100 mm
Al_2O_3	−0.10/0.47	−6.83/5.48	−18.3/0.01	−20.8/1.92	−28.4/0.00	−28.5/0.11
HfO_2	0.00/46.4	−0.68/39.1	−3.57/0.12	−10.5/5.44	−30.4/0.00	−31.2/0.59
Nb_2O_5	−0.01/21.5	−1.25/18.0	−10.5/0.06	−14.9/3.43	−27.7/0.00	−28.1/032
SiO_2	0.00/17.0	−0.14/14.4	−0.02/0.51	−1.86/1.81	−8.43/0.00	−8.69/0.21
Ta_2O_5	0.00/27.6	−0.96/23.1	−8.21/0.07	−13.1/3.86	−27.5/0.00	−27.9/0.38
Al_2O_3–SiO_2	0.00/9.44	−1.09/8.05	−8.10/0.03	−10.5/1.86	−17.5/0.00	−17.7/0.16
HfO_2–SiO_2	0.00/29.2	−0.36/24.6	−1.21/0.07	−5.43/3.31	−17.5/0.00	−18.0/0.36

representative of the full-size optic's behavior. Instead of using only a test sample or witness as the sole predictor of the thermal stress response of a large part, the additional use of a thermomechanical model as described in this paper (as a supplementary tool) may improve outcomes by alerting process developers to possible coating stress issues for the cleaning process that are unique to large optics.

5. Conclusions

A thermomechanical model was developed and used to estimate the stress response of oxide coatings to elevated-temperature wet processing. Results indicate that substrate geometry strongly affects the thermal stress response of the thin-film material. An oxide coating on a thin substrate generally exhibited *either* tensile or compressive stresses during elevated temperature processing, depending on the CTE mismatch between substrate and coating. In the case of a thick substrate, however, the thin-film coating was likely to exhibit *both* compressive and tensile stresses during its processing history. The substrate-thickness effect was more important for some combinations of coating and substrate than others; for some combinations (e.g., a hafnia–silica MLD coating on a fused-silica substrate), the coating had nearly the same stress response for 10 and 100 mm substrate thicknesses. These results suggest that special consideration must be paid to geometry in the selection of small-scale witness/test materials to model the response of large optics to thermal processing.

The model was used to investigate the thermal stresses developed during elevated-temperature cleaning of a hafnia–silica OMEGA EP pulse compression grating. Piranha cleaning at 100°C (60 min heating and cooling ramps, 30 min soak) led to substrate stresses in the range of −15.7 to +11.8 MPa and coating stresses in the range of −0.7 to +49.3 MPa for a 100-mm-thick BK7 substrate. These high stresses suggest that an OMEGA EP grating would be susceptible to both coating failure and substrate fracture during cleaning, highlighting the importance of gentle, low-temperature cleaning. For a 40°C cleaning process with an optimized heating rate of 1°C/min, substrate stresses were predicted to be in the range of −6.6 to +5.0 MPa and coating stresses in the range of −0.51 to +11.0 MPa. Failure of the coating or substrate would not be expected at these levels.

The authors thank Ms. Brittany Taylor, Mr. Justin Dressler, and Mr. Chase Quintana for their work in imaging the defects shown in Fig. 2 in Nomarski microscopy. H. P. H. L. acknowledges support through a Horton fellowship at the Laboratory for Laser Energetics. This material is based upon work supported by the U.S. Department of Energy under Award DE-EE0006033.000 and by the Department of Energy National Nuclear Security Administration under Award DE-NA0001944.

References

1. B. Ashe, C. Giacofei, G. Myhre, and A. W. Schmid, "Optimizing a cleaning process for multilayer dielectric (MLD) diffraction gratings," Proc. SPIE **6720**, 67200N (2007).
2. H. P. Howard, A. F. Aiello, J. G. Dressler, N. R. Edwards, T. J. Kessler, A. A. Kozlov, I. R. T. Manwaring, K. L. Marshall, J. B. Oliver, S. Papernov, A. L. Rigatti, A. N. Roux, A. W. Schmid, N. P. Slaney, C. C. Smith, B. N. Taylor, and S. D. Jacobs, "Improving the performance of high-laser-damage-threshold, multilayer dielectric pulse-compression gratings through low-temperature chemical cleaning," Appl. Opt. **52**, 1682–1692 (2013).
3. S. Chen, B. Sheng, X. Xu, and S. Fu, "Wet-cleaning of contaminants on the surface of multilayer dielectric pulse compressor gratings by the Piranha solution," Proc. SPIE **7655**, 765522 (2010).
4. S. Chen, B. Sheng, K. Qui, Z. Liu, X. Xu, Y. Liu, Y. Hong, and F. Shaojun, "Cleaning multilayer dielectric pulse compressor gratings with top layer of HfO_2 by Piranha solution," High Power Laser Part. Beams **23**, 2106–2110 (2011).
5. B. Ashe, K. L. Marshall, C. Giacofei, A. L. Rigatti, T. J. Kessler, A. W. Schmid, J. B. Oliver, J. Keck, and A. Kozlov, "Evaluation of cleaning methods for multilayer diffraction gratings," Proc. SPIE **6403**, 64030O (2007).
6. H. P. H. Liddell, K. Mehrotra, J. C. Lambropoulos, and S. D. Jacobs, "Fracture mechanics of delamination defects in multilayer dielectric coatings," Appl. Opt. **52**, 7689–7698 (2013).
7. J. W. Hutchinson and Z. Suo, "Mixed mode cracking in layered materials," in *Advances in Applied Mechanics*, J. W. Hutchinson and T. Y. Wu, eds. (Academic, 1992), Vol. **29**, pp. 63–191.
8. B. A. Boley and J. H. Weiner, *Theory of Thermal Stresses* (Dover Publications, 1997), pp. 195–239.
9. M. N. Özisik, *Heat Conduction* (Wiley, 1980), pp. 259–262.
10. B. A. Boley and J. H. Weiner, *Theory of Thermal Stresses* (Dover Publications, 1997), pp. 277–287.
11. J. B. Oliver, P. Kupinski, A. L. Rigatti, A. W. Schmid, J. C. Lambropoulos, S. Papernov, A. Kozlov, C. Smith, and R. D. Hand, "Stress compensation in hafnia/silica optical coatings by inclusion of alumina layers," Opt. Express **20**, 16596–16610 (2012).
12. D. J. Smith, M. McCullough, C. Smith, T. Mikami, and T. Jitsuno, "Low stress ion-assisted coatings on fused silica substrates for large aperture laser pulse compression gratings," Proc. SPIE **7132**, 71320E (2008).
13. J. B. Oliver, P. Kupinski, A. L. Rigatti, A. W. Schmid, J. C. Lambropoulos, S. Papernov, A. Kozlov, J. Spaulding, D. Sadowski, Z. R. Chrzan, R. D. Hand, D. R. Gibson, I. Brinkley, and F. Placido, "Large-aperture plasma-assisted deposition of inertial confinement fusion laser coatings," Appl. Opt. **50**, C19–C26 (2011).
14. Optical Glass Data Sheets, Schott N-BK7, Schott North America, available at http://www.schott.com/advanced_optics/us/abbe_datasheets/schott_datasheet_all_us.pdf.
15. Ľ. Kubičár, V. Vretenár, and U. Hammerschmidt, "Thermophysical parameters of optical glass BK7 measured by the pulse transient method," Int. J. Thermophys. **26**, 507–518 (2005).
16. Corning Semiconductor Optics: HPFS Fused Silica Standard Grade, available at http://www.corning.com/docs/specialtymaterials/pisheets/H0607_hpfs_Standard_ProductSheet.pdf.
17. Optical Glass Data Sheets, Schott Borofloat 33, Schott North America, available at http://www.us.schott.com/borofloat/english/download/borofloat33_gen_us_web.pdf.
18. H. H. Friis-Pedersen, J. H. Pedersen, L. C. Hausslerb, and B. K. Storm, "Online measurement of thermal diffusivity during cure of an epoxy composite," Polymer Testing **25**, 1059–1068 (2006).
19. R. Thielsch, A. Gatto, and N. Kaiser, "Mechanical stress and thermal-elastic properties of oxide coatings for use in the deep-ultraviolet spectral region," Appl. Opt. **41**, 3211–3217 (2002).

20. E. Çetinörgü, B. Baloukas, O. Zabeida, J. E. Klemberg-Sapieha, and L. Martinu, "Mechanical and thermoelastic characteristics of optical thin films deposited by dual ion beam sputtering," Appl. Opt. **48**, 4536–4544 (2009).
21. H. Liu, "Thermal stress fracture of optical glasses," Ph.D. thesis (University of Rochester, 2010).
22. A. L. Rigatti and D. J. Smith, "Status of optics on the OMEGA laser after 18 months of operation," Proc. SPIE **2966**, 441–450 (1997).
23. J. H. Campbell, P. A. Hurst, D. D. Heggins, W. A. Steele, and S. E. Bumpas, "Laser induced damage and fracture in fused silica vacuum windows," Proc. SPIE **2966**, 106–125 (1997).
24. J. C. Lambropoulos, T. Fang, P. D. Funkenbusch, S. D. Jacobs, M. J. Cumbo, and D. Golini, "Surface microroughness of optical glasses under deterministic microgrinding," Appl. Opt. **35**, 4448–4462 (1996).
25. "Slow crack growth during radiative cooling of LHG8 and BK7 plates," LLE Document No. DOE/NA/28302-900, LLE Review Quarterly Report 119 (Laboratory for Laser Energetics, University of Rochester, 2009), pp. 145–153.
26. H. Leplan, B. Geenen, J. Y. Robic, and Y. Pauleau, "Residual stresses in evaporated silicon dioxide thin films: correlation with deposition parameters and aging behavior," J. Appl. Phys. **78**, 962–968 (1995).
27. J. B. Oliver, "Evaporated HfO_2/SiO_2 optical coatings and modifications for high-power laser applications," Ph.D. thesis (University of Rochester, 2012).
28. F. Kong, S. Chen, S. Liu, Y. Jin, H. Guan, Y. Du, C. Wei, H. He, and K. Yi, "Laser-induced damage of multilayer dielectric for broadband pulse compression grating," Proc. SPIE **8206**, 82060P (2011).